BJP British Journal of Pharmacology

DOI:10.1111/bph.12842
www.brjpharmacol.org

RESEARCH PAPER

Determination of the binding mode for the cyclopentapeptide CXCR4 antagonist FC131 using a dual approach of ligand modifications and receptor mutagenesis

S Thiele[1]*, J Mungalpara[2]*, A Steen[1], M M Rosenkilde[1] and J Våbenø[2]

[1]*Laboratory for Molecular Pharmacology, Department of Neuroscience and Pharmacology, Faculty of Health and Medical Sciences, The Panum Institute, University of Copenhagen, Copenhagen, Denmark, and* [2]*Department of Pharmacy, Faculty of Health Sciences, UiT The Arctic University of Norway, Tromsø, Norway*

Correspondence
Mette Marie Rosenkilde, Laboratory for Molecular Pharmacology, Department of Neuroscience and Pharmacology, Faculty of Health and Medical Sciences, The Panum Institute, University of Copenhagen, Blegdamsvej 3, DK-2200 Copenhagen, Denmark. E-mail: rosenkilde@sund.ku.dk. Jon Våbenø, Department of Pharmacy, Faculty of Health Sciences, UiT The Arctic University of Norway, Breivika, NO-9037 Tromsø, Norway. E-mail: jon.vabeno@uit.no

*These authors contributed equally as first authors.

Received
9 January 2014
Revised
25 June 2014
Accepted
8 July 2014

BACKGROUND AND PURPOSE

The cyclopentapeptide FC131 (cyclo(-L-Arg[1]-L-Arg[2]-L-2-Nal[3]-Gly[4]-D-Tyr[5]-)) is an antagonist at the CXC chemokine receptor CXCR4, which plays a role in human immunodeficiency virus infection, cancer and stem cell recruitment. Binding modes for FC131 in CXCR4 have previously been suggested based on molecular docking guided by structure–activity relationship (SAR) data; however, none of these have been verified by *in vitro* experiments.

EXPERIMENTAL APPROACH

Heterologous ^{125}I-12G5-competition binding and functional assays (inhibition of CXCL12-mediated activation) of FC131 and three analogues were performed on wild-type CXCR4 and 25 receptor mutants. Computational modelling was used to rationalize the experimental data.

KEY RESULTS

The Arg[2] and 2-Nal[3] side chains of FC131 interact with residues in TM-3 (His[113], Asp[171]) and TM-5 (hydrophobic pocket) respectively. Arg[1] forms charge-charge interactions with Asp[187] in ECL-2, while D-Tyr[5] points to the extracellular side of CXCR4. Furthermore, the backbone of FC131 interacts with the chemokine receptor-conserved Glu[288] via two water molecules. Intriguingly, Tyr[116] and Glu[288] form a H-bond in CXCR4 crystal structures and mutation of either residue to Ala abolishes CXCR4 activity.

CONCLUSIONS AND IMPLICATIONS

Ligand modification, receptor mutagenesis and computational modelling approaches were used to identify the binding mode of FC131 in CXCR4, which was in agreement with binding modes suggested from previous SAR studies. Furthermore, insights into the mechanism for CXCR4 activation by CXCL12 were gained. The combined findings will facilitate future design of novel CXCR4 antagonists.

Abbreviations

2-Nal, 3-(2-naphthyl)alanine; 7TM, 7 transmembrane helix; Aib, 2-aminoisobutyric acid; Cit, citrulline; ECL, extracellular loop; HIV, human immunodeficiency virus; IP, inositol phosphate; SAR, structure–activity relationship; WT, wild type

Tables of Links

TARGETS	LIGANDS
CCR2 chemokine receptor	AMD3100 (plerixafor)
CCR5 chemokine receptor	Aplaviroc
CXCR4 chemokine receptor	CXCL12
EBI2 (GPR183)	T140

This Table lists key protein targets and ligands in this article which are hyperlinked to corresponding entries in http://www.guidetopharmacology.org, the common portal for data from the IUPHAR/BPS Guide to PHARMACOLOGY (Pawson *et al.*, 2014) and are permanently archived in the Concise Guide to PHARMACOLOGY 2013/14 (Alexander *et al.*, 2013).

Introduction

The chemokine receptor CXCR4 belongs to the class A 7-transmembrane helix (7TM) receptors, also known as GPCRs. It plays a role in human immunodeficiency virus (HIV) infection by being a cell-entry co-factor for T-cell tropic HIV strains (Berson *et al.*, 1996; Feng *et al.*, 1996), and is together with its endogenous agonist CXCL12, central for stem cell recruitment and cancer development, progression, and metastasis (Murphy *et al.*, 2000; Balkwill, 2004; Bachelerie *et al.*, 2014). These implications have facilitated the development of drug candidates targeting CXCR4 (Choi *et al.*, 2012). One of these, the bicyclam compound AMD3100 (plerixafor), was approved in 2008 for haematopoietic stem cell mobilization in patients with multiple myeloma and non-Hodgkin's lymphoma (DiPersio *et al.*, 2009a,b; Micallef *et al.*, 2009), although the initial indication was as an anti-HIV compound (De Clercq *et al.*, 1994; Steen *et al.*, 2009).

The polyphemusin II-derived peptides are a large class of CXCR4 antagonists that include the 14-mer T140 (Tamamura *et al.*, 1998) and analogues, for example, CVX15 (Wu *et al.*, 2010), as well as the cyclic pentapeptide FC131 (Figure 1A) and analogues (Fujii *et al.*, 2003). The cyclopentapeptide CXCR4 antagonists were designed by combining the four most important residues of T140 (Arg^2, $2\text{-}Nal^3$, $D\text{-}Tyr^5$ and Arg^{14}) with a Gly residue to give a cyclopentapeptide library (Tamamura *et al.*, 2000; Fujii *et al.*, 2003). The optimal combination of sequence and stereochemistry was shown to be cyclo(-L-Arg^1-L-Arg^2-L-2-Nal^3-Gly^4-D-Tyr^5-), that is, FC131, which displays nanomolar affinity and potency at CXCR4 (Fujii *et al.*, 2003) and serves as lead compound for development of more drug-like peptidomimetic CXCR4 antagonists. Structure–activity relationship (SAR) studies of FC131 have shown that although a positive charge is preferred at position 1, substitution of Arg^1 with the uncharged citrulline (Cit), or even less structurally related amino acids, is tolerated (Tamamura *et al.*, 2005a; Demmer *et al.*, 2011; Mungalpara *et al.*, 2012). In contrast, Arg^2 is a crucial functionality and minor modifications abolish activity (Tamamura *et al.*, 2005b; Demmer *et al.*, 2011; Mungalpara *et al.*, 2012). The aromatic residues in positions 3 ($2\text{-}Nal^3$) and 5 ($D\text{-}Tyr^5$) are also important for proper function; importantly, position 3 requires conservation as 2-Nal (Tamamura *et al.*, 2005b; Mungalpara *et al.*, 2013) while position 5 allows for some modifications (Tamamura *et al.*, 2005b; Tanaka *et al.*, 2009; Mungalpara *et al.*, 2013).

Several computational models for binding of peptide antagonists to CXCR4 have been suggested. The first models for T140 (Trent *et al.*, 2003) and FC131 (Våbenø *et al.*, 2006a; Kawatkar *et al.*, 2011) were based on the crystal structure of bovine rhodopsin (Palczewski *et al.*, 2000); however, the subsequent publication of the crystal structures of CXCR4 (Wu *et al.*, 2010) revealed significant structural differences between rhodopsin and CXCR4. The co-crystal complex between CXCR4 and CVX15, a 16-mer analogue of T140, also showed that peptide CXCR4 antagonists bind differently than previously suggested. Based on molecular docking to this crystal structure, guided by SAR data, more reliable binding models have since emerged for the cyclopentapeptide antagonists (Demmer *et al.*, 2011; Kobayashi *et al.*, 2012; Mungalpara *et al.*, 2012; 2013; Yoshikawa *et al.*, 2012). These models collectively suggest an interaction between Arg^1 of FC131 and Asp^{187} (in ECL-2) and Asp^{97} in TM-2, while Arg^2 interacts with His^{113} (TM-3) and Asp^{171} (TM-4). [The position of residues according to the Baldwin/Schwartz (Schwartz, 1994; Baldwin *et al.*, 1997) and the Ballesteros/Weinstein numbering system (Ballesteros and Weinstein, 1995) is given in the tables.] Furthermore, the $2\text{-}Nal^3$ side chain is located in a hydrophobic pocket facing TM-5, while $D\text{-}Tyr^5$ is proposed to interact with either Glu^{32} in the N-terminus, Tyr^{45} in TM-1, or aromatic residues in ECL-2. Moreover, the chemokine receptor-conserved Glu^{288}, a residue often involved in binding of positively charged small-molecule ligands (Rosenkilde and Schwartz, 2006), is suggested to interact indirectly with FC131 via water molecules (Mungalpara *et al.*, 2012; Yoshikawa *et al.*, 2012). Thus, in line with reported SAR for FC131, the crucial Arg^2 and $2\text{-}Nal^3$ side chains bind deep in the receptor main binding crevice, while the less important Arg^1 and $D\text{-}Tyr^5$ side chains experience a larger degree of conformational flexibility and are partly solvent exposed, facing the extracellular surface of the receptor (Mungalpara *et al.*, 2013). However, none of these computational models have been accompanied by *in vitro* experiments that verify the suggested binding modes.

To determine the binding mode for the lead cyclopentapeptide CXCR4 antagonist FC131, we here report experimental studies that involve modifications of both receptor and ligand. Thus, FC131 and the three analogues [Cit^1]FC131

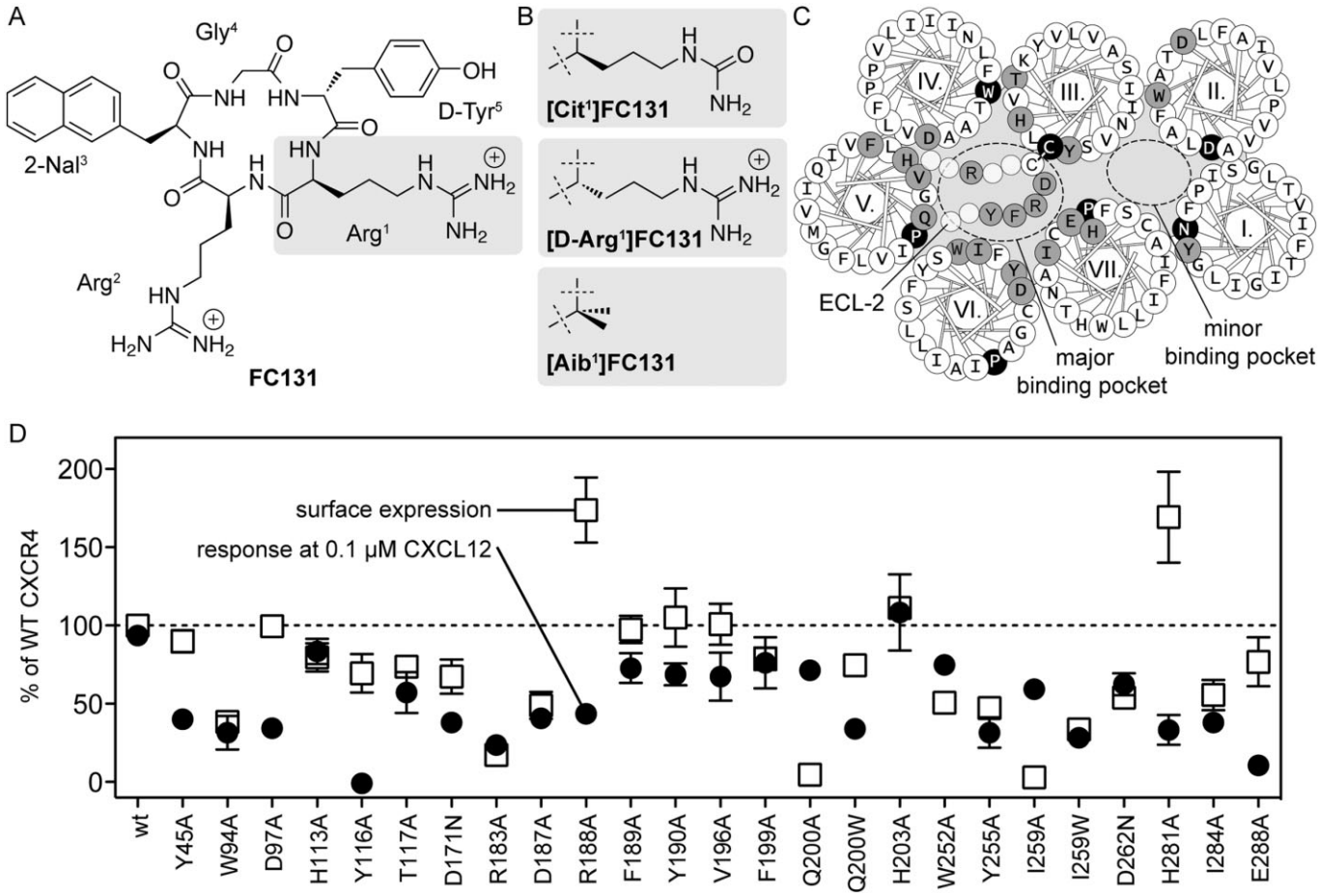

Figure 1

Compounds and mutations included in this study. (A) Structure of FC131 and (B) analogues [Cit[1]]FC131, [Aib[1]]FC131 and [D-Arg[1]]FC131, for which only the structure of the modified side chain 1 is shown. (C) Helical wheel diagram of CXCR4 as seen from the extracellular side showing the upper halves of the TMs and parts of ECL-2. Residues with black background are conserved among class A GPCRs and residues on grey background were mutated in this study. (D) Surface expression and response to 0.1 µM CXCL12 in functional assay of each mutant.

(substitution of the positively charged L-Arg in position 1 with the neutral L-Cit), [Aib[1]]FC131 (substitution of Arg[1] with the small hydrophobic 2-aminoisobutyric acid) and [D-Arg[1]]FC131 (opposite stereochemistry in position 1) (Figure 1B) were tested in a library of 25 CXCR4 mutations including Ala, Asn or Trp substitutions of residues in TM-1 to -7 and ECL-2 (Figure 1C) in ^{125}I-12G5-binding and receptor-activation assays. This combined approach is the first of its kind to directly investigate the binding mode for FC131 in CXCR4 with *in vitro* experiments. Interestingly, the receptor mutagenesis also revealed residues important for CXCL12-induced receptor activation. The combined findings provide new experimental insight into the molecular mechanisms of CXCR4 antagonism and will facilitate future design of novel CXCR4 antagonists.

Methods

Compounds

Complete details of the synthesis and characterization of the cyclopentapeptide ligands FC131, [Cit[1]]FC131, [Aib[1]]FC131 and [D-Arg[1]]FC131 have been reported earlier (Mungalpara *et al.*, 2012).

Site-directed mutagenesis

Receptor mutations were introduced by the polymerase chain reaction overlap extension technique or the QuikChange technique (Agilent Technologies, Santa Clara, CA, USA) using wild-type (WT) CXCR4 as template. All reactions were carried out using Pfu polymerase (Stratagene, La Jolla, CA, USA) under conditions recommended by the manufacturer. The mutations were cloned into the eukaryotic expression vector pcDNA3.1+ (Invitrogen, Carlsbad, CA, USA) and verified by restriction endonuclease digestion and DNA sequencing (Eurofins MWG Operon, Ebersberg, Germany).

Transfections and tissue culture

COS-7 cells were grown in DMEM with Glutamax (Invitrogen) supplemented with 10% FBS, 180 U·mL^{-1} penicillin and 45 µg·mL^{-1} streptomycin at 37°C in a 10% CO_2/90% air-humidified atmosphere. Transfection of cells was carried out by the calcium phosphate precipitation method (Rosenkilde

et al., 1994; Kissow *et al.*, 2012). Briefly, plasmid DNA (20 μg of receptor cDNA and 30 μg of the chimeric G-protein $G\alpha_{qi4myr}$ for inositol phosphate (IP) assays, or 40 μg receptor cDNA for ^{125}I-12G5-binding assays) was mixed with TE buffer (10 mM Tris-HCl, 2 mM EDTA-Na_2, pH 7.5) and 30 μL calcium chloride (2 M) to a total volume of 480 μL, and was then added to the same amount of HEPES buffered saline (280 mM NaCl, 50 mM HEPES, 1.5 mM Na_2HPO_4, pH 7.2). Precipitation was allowed for 45 min at room temperature, after which the precipitate, together with 300 μL chloroquine (2 mg·mL^{-1}) in 10 mL culture media, was added to the 6×10^6 COS-7 cells seeded the day before. Transfection was stopped after 5 h by replacing media and cells were incubated overnight.

Functional assay

The potency was measured using IP accumulation assays. In brief, 1 day after transfection, COS-7 cells (1.5×10^5 cells/well) were incubated for 24 h with 2 μCi of [^{3}H]-myo-inositol in 0.3 mL of growth medium per well in a 24-well plate. The following day, cells were washed twice in PBS and were incubated in 0.2 mL of Hank's balanced salt solution (Invitrogen) supplemented with 10 mM LiCl at 37°C in the presence of various concentrations of ligands for 90 min. All mutations were tested for their ability to become activated by CXCL12 using concentrations from 10 pM to 0.1 μM. The IC_{50} of the antagonists was determined in cells activated by CXCL12 to approximately 80% of CXCL12 E_{max}. The antagonists (in a range from 1 nM to 100 μM) were added 10 min prior to addition of CXCL12, and co-incubated with CXCL12 for 90 min. Assay medium was then removed, and cells were extracted by addition of 1 mL of 10 mM formic acid to each well, followed by incubation on ice for 30–60 min. The generated [^{3}H]IPs were purified on an AG 1-X8 anion exchange resin. After addition of multipurpose liquid scintillation cocktail (Gold Star, Triskem-International, Bruz, France), radiation was counted in a Beckman Coulter counter LS6500 (Beckman Coulter Danmark ApS c/o OptiNordic ApS, Copenhagen, Denmark). As an alternative assay measuring IP accumulation, the SPA-IP was sometimes used. In brief, 1 day after transfection, COS-7 cells (35.000 cells/well) were incubated with [^{3}H]myo-inositol (5 μL·mL^{-1}, 2 μCi·mL^{-1}) in 0.1 mL of media overnight in a 96-well plate. The next day, cells were treated as mentioned above with volumes adjusted as follows: 100 μL of reaction solution with LiCl and 50 μL ice-cold formic acid (10 mM, 50 μL/well). The [^{3}H]IPs in the formic acid cell lysates were thereafter quantified by Ysi-poly-D-Lys-coated SPA beads. Briefly, 20 μL of cell extract was mixed with 80 μL of SPA bead suspension in H_2O (12.5 μg·μL^{-1}) to give a final volume of 100 μL in a PicoPlate-96 white plate. Plates were sealed, agitated for at least 30 min and centrifuged (5 min, 402 rcf). SPA beads were allowed to settle and react with the extract for 8 h before radioactivity was determined using a Packard Top Count NXT™ scintillation counter (Perkin Elmer). All determinations were made in duplicate. These overall readouts have earlier been used effectively for CXCR4 and other chemokine receptors and were found to give comparable results (Brandish *et al.*, 2003; Mungalpara *et al.*, 2012; Thiele *et al.*, 2012).

Binding experiments

Cells were transfected as described above. The number of cells seeded per well was determined by the apparent receptor expression efficiency and was aimed at obtaining 5–10% specific binding of the added radioactive ligand. Two days after transfection, cells were assayed by competition binding for 3 h at 4°C using 10–15 pM ^{125}I-12G5 plus unlabelled ligand in 0.2 mL (in 24-well plates, up to 150.000 cells/well) or 0.1 mL (96-well plates, up to 35.000 cells/well) of 50 mM HEPES buffer, pH 7.4, supplemented with 1 mM $CaCl_2$, 5 mM $MgCl_2$ and 0.5% (w/v) BSA in 24-well plates. The binding of ^{125}I-12G5 was competed for with increasing concentrations of the unlabelled ligand ranging from 10 pM to 100 nM (12G5) or from 1 nM to 100 μM (FC131, [Cit^1]FC131, [Aib^1]FC131 or [D-Arg^1]FC131). After incubation, cells were washed quickly two times in 4°C binding buffer supplemented with 0.5 M NaCl. Cells were lysed by addition of 0.5 mL carbamide solution (18% acetic acid, 8 M urea, 2% v/v P-40) and radioactivity was counted in a WALLAC Wizard Gamma Counter (Perkin Elmer). Non-specific binding was determined in the presence of 0.1 μM unlabelled 12G5. Determinations were made in duplicate.

ELISA

COS-7 cells were seeded in 96-well plates (6×10^3 cells/well) and transfected with 12.5 ng/well N-terminally FLAG-tagged receptor DNA using lipofectamine transfection according to manufacturer's instructions (Invitrogen). Two days after transfection, cells were washed in Tris-buffered saline (TBS; 0.05 M Tris Base, 0.9% NaCl, pH 7.6), fixed in 3.7% formaldehyde for 15 min at room temperature, washed three times in TBS, and incubated in TBS with 2% BSA for 30 min. The cells were then incubated for 2 h with anti-FLAG M1-antibody (Sigma-Aldrich, St. Louis, MO, USA) at 2 μg·mL^{-1} in TBS with 1 mM $CaCl_2$ and 1% BSA. After three washes with TBS supplemented with 1 mM $CaCl_2$, the cells were incubated with goat anti-mouse HRP-conjugated antibody at 0.8 μg·mL^{-1} (Thermo Fisher Scientific, Waltham, MA, USA) for 1 h. The immunoreactivity was revealed by addition of TMB Plus substrate (Kem-En-Tec, Taastrup, Denmark) after three additional washes, and the reaction was stopped with 0.2 M H_2SO_4. Absorbance was measured at 450 nm on a Wallac Envision 2104 Multilabel Reader (Perkin Elmer).

Molecular docking

Docking of the cyclopentapeptide ligands to the CXCR4 receptor was performed as described earlier (Mungalpara *et al.*, 2012). Briefly, the X-ray structure of human CXCR4 (bound to CVX15, PDB code 3OE0) (Wu *et al.*, 2010) was prepared with the Protein Preparation Wizard workflow (Schrödinger Suite 2011 Protein Preparation Wizard; Epik version 2.2, Schrödinger, LLC, New York, NY, USA; Impact version 5.7, Schrödinger, LLC; Prime version 2.3, Schrödinger, LLC), and our previously reported bioactive backbone conformation for FC131 (Våbenø *et al.*, 2006b) was used to build the structure of the cyclopentapeptide ligands. The ligands were docked using Schrödingers induced-fit docking workflow (Schrödinger Suite 2012 Induced Fit

Docking protocol; Glide version 5.8, Schrödinger, LLC; Prime version 3.1, Schrödinger, LLC), which takes the conformational flexibility of both ligand and receptor residues into account. Asp^{187} was used as centroid for the docking box (a cube with 26 Å length) and a H-bond constraint was applied to the carboxylate oxygen atoms of Asp^{171}. As the side chain of Arg^{188} partly restricted access to Asp^{171}, the 'trim' option was used for Arg^{188}, that is, the side chain is replaced with a methyl group (alanine) in the initial docking step and then placed back in the final redocking step. For all four ligands, 100 initial poses were generated, and the top 10 optimized poses were retrieved.

Data analysis

Statistical analyses were performed using the GraphPad Prism 5 software (GraphPad Software, San Diego, CA, USA). The EC_{50} and IC_{50} values represent the mean of at least three independent experiments (except for [Cit^1]FC131 and [Aib^1]FC131 in 125G binding to Y116A) performed in duplicate (for exact number of experiments, see tables). In cases of incomplete sigmoidal curves (plateau not reached), the curves were extrapolated to baselines (see below) to predict an EC_{50} or IC_{50}. If this seemed unjustified, logEC_{50}/IC_{50} values were indicated as >–4 or >–7 in the tables. *P*-values were calculated using unpaired two-tailed *t*-test with 95% confidence intervals. Dose–response curves represent averaged, normalized curves. The normalizations were done as follows. (i) In the functional assay, cells were activated to approximately 80% by addition of an appropriate concentration of CXCL12 (see section on functional assay). This activation was set to 100% in each individual experiment, while the background response observed for transfected cells in the absence of ligand was set to 0%. The average of these normalized curves for each assay ('row means' in Prism 5) was then calculated. (ii) In the ^{125}I-12G5-binding assays, 100% equals maximum ^{125}I-12G5 binding to receptor-expressing cells in the absence of unlabelled ligand, while 0% equals the unspecific binding observed with 0.1 μM 12G5.

Materials

All reagents and solvents were purchased and used as received without further purification. The human chemokine CXCL12 was purchased from PeproTech (Rocky Hill, NJ, USA). Human CXCR4 receptor cDNA was kindly provided by Timothy NC Wells (GSK, Brentford, UK). [^{3}H]-myo-inositol (PT6-271), scintillation proximity assay (SPA) beads and ^{125}I-Bolton-Hunter reagent were purchased from Perkin Elmer (Waltham, MA, USA). A 12G5 antibody was kindly provided by Jim Hoxie (University of Pennsylvania, Philadelphia, PA, USA) and was iodinated in house as described previously (Rosenkilde *et al.*, 2004). cDNA for the promiscuous chimeric G-protein $G_{\Delta 6qi4myr}$ (abbreviated G_{qi4myr}) was kindly provided by Evi Kostenis (University of Bonn, Germany) (Kostenis *et al.*, 1998). Primers for mutations were bought from TAG Copenhagen (Denmark). The stock solution and dilutions of peptide antagonists were made in water. Stock solution and all dilutions of CXCL12 were made in buffer (1 mM acetic acid + 0.1% BSA).

Results

Expression and functionality of mutant receptors

A library of 25 CXCR4 mutations with Ala, Asn and steric hindrance substitutions of residues located in TM-1 to -7 and ECL-2 (Figure 1C) was created based on previously suggested binding modes of FC131 (Demmer *et al.*, 2011; Mungalpara *et al.*, 2012; Yoshikawa *et al.*, 2012) and the ability of the residues to engage in H-bond, charge-charge and hydrophobic interactions. Thus, these residues constituted likely interaction sites for the main functionalities of FC131, that is, the positively charged side chains of Arg^1 and Arg^2, the aromatic side chains of 2-Nal^3 and D-Tyr^5, and the peptide backbone.

Initially, WT CXCR4 and all mutant receptors were tested for their surface expression using ELISA, and for their functional response towards the endogenous chemokine CXCL12 using COS-7 cells transiently transfected with receptor and the $G\alpha_i$- to $G\alpha_q$-signal-converting chimeric G_α subunit G_{qi4myr}, thus measuring accumulation of intracellular IP (Table 1, Figure 1D). The majority of receptors displayed expression levels from 47 to 111% of WT. R183A, I259W and W94A ranged at the lower end of the scale with 18, 34 and 39% of WT expression, respectively, while two receptors (R188A and H281A) showed expression levels higher than 130% compared with WT (Table 1). I259A and Q200A displayed the lowest expression with 4.7 and 3.0% of WT level; however, both receptors showed good responses towards CXCL12, demonstrating that they were functional and correctly folded. Likewise, the majority of the receptors showed good responses towards CXCL12 (Table 1, Figure 1D). Only W94A, D97A and D187A resulted in 8.6- to 14-fold decreased potencies compared with WT CXCR4, and no response was observed for Y116A and E288A (discussed below), despite good surface expression (Table 1, Figure 1D).

Nine mutations were also assessed in ^{125}I-12G5-competition binding experiments in transiently transfected COS-7 cells (Table 2). This assay has earlier been shown to correlate better with HIV-1 antiviral potency of CXCR4 antagonists than functional assays measuring CXCR4 signalling, and also displays a larger dynamic range (Gerlach *et al.*, 2003; Rosenkilde *et al.*, 2007). These selected receptors were able to bind 12G5 with WT-like affinities (1.9–16 nM) (Table 2). The B_{max} values were slightly, yet significantly, reduced for H113A, D171N, H281A and E288A (Table 2), which however did not correlate to their WT-like surface expression (Table 1).

While secondary/global effects of the mutations on receptor structure and function cannot be excluded, the created set of receptor mutants was deemed suitable for mapping the binding site of FC131 by assessing its ability to inhibit CXCL12-mediated activation or to displace ^{125}I-12G5.

FC131-mediated inhibition of CXCL12-induced receptor activation

The entire mutant library was tested in a functional assay determining the ability of the cyclopentapeptide antagonist FC131 to inhibit CXCL12-induced accumulation of intracellular IP. H113A, D171N and D262N in the major binding pocket resulted in 12- to 119-fold reduced FC131 potencies

Table 1

Functional analysis of the interaction between CXCR4 WT and mutants with CXCL12, FC131 and analogues

Receptor			Surface expression		CXCL12					FC131			
Helix	Position	Mutation	% ± SEM	(*n*)	EC_{50} ± SEM (log)	EC_{50} (nM)	F_{mut}	Response at 0.1 μM % of WT ± SEM	(*n*)	EC_{50} ± SEM (log)	EC_{50} (μM)	F_{mut}	(*n*)
WT	WT	WT[a]	100 ± 0.0	(5)	−8.8 ± 0.04	1.5	1.0	94 ± 1.3	(69)	−6.4 ± 0.04	0.40	1.0	(31)
TM-1	I:07/1.39	Y45A	90 ± 7.0	(3)	−8.5 ± 0.20	3.4	2.3**	40 ± 5.5	(10)	−5.8 ± 0.09	1.6	4.1***	(6)
TM-2	II:20/2.60	W94A[a]	38 ± 6.4	(3)	−7.7 ± 0.10	18	*13***	31 ± 11	(17)	−8.0 ± 0.30	0.01	0.03***	(8)
	II:23/2.63	D97A[a]	99 ± 6.3	(4)	−7.7 ± 0.07	20	*14***	34 ± 3.5	(10)	−7.4 ± 0.09	0.04	0.11***	(5)
TM-3	III:05/3.29	H113A[a]	80 ± 9.0	(3)	−9.1 ± 0.08	0.84	0.58**	83 ± 8.1	(21)	−4.3 ± 0.10	48	**119*****	(11)
	III:08/3.32	Y116A[a]	69 ± 12	(3)	**No activation**			−0.8 ± 5.9	(5)	Not determined			
	III:09/3.33	T117A	74 ± 5.5	(3)	−8.8 ± 0.09	1.7	1.2	57 ± 13	(4)	−6.9 ± 0.05	0.14	0.34**	(3)
TM-4	IV:20/4.60	D171N[a]	67 ± 11	(3)	−8.5 ± 0.08	3.2	2.2***	38 ± 4.7	(25)	−5.3 ± 0.12	4.6	*12****	(13)
	ECL-2/Cys-3	R183A	17 ± 1.8	(3)	−10 ± 0.20	0.10	0.07***	24 ± 1.4	(3)	−6.3 ± 0.18	0.49	1.2	(3)
ECL-2	ECL-2/Cys+1	D187A[a]	49 ± 8.7	(4)	−7.9 ± 0.06	13	*8.6****	41 ± 5.2	(3)	−6.9 ± 0.02	0.14	0.35***	(3)
	ECL-2/Cys+2	R188A	174 ± 21	(3)	−9.3 ± 0.08	0.53	0.36**	44 ± 3.5	(4)	−6.1 ± 0.17	0.72	1.8	(3)
	ECL-2/Cys+3	F189A	97 ± 8.7	(3)	−8.7 ± 0.11	1.8	1.2	73 ± 9.5	(9)	−7.0 ± 0.20	0.10	0.25***	(6)
	ECL-2/Cys+4	Y190A	105 ± 19	(3)	−8.9 ± 0.18	1.2	0.82	69 ± 7.0	(8)	−6.3 ± 0.24	0.47	1.2	(5)
TM-5	V:01/5.35	V196A	101 ± 13	(3)	−8.9 ± 0.17	1.4	0.96	67 ± 15	(8)	−6.3 ± 0.04	0.47	1.2	(4)
	V:04/5.38	F199A	79 ± 7.2	(3)	−8.8 ± 0.06	1.4	0.98	76 ± 16	(4)	−6.7 ± 0.11	0.21	0.52*	(4)
	V:05/5.39	Q200A	4.7 ± 2.8	(3)	−8.9 ± 0.07	1.4	0.95	71 ± 5.1	(10)	−6.4 ± 0.13	0.36	0.89	(5)
	V:05/5.39	Q200W	75 ± 5.2	(3)	−8.7 ± 0.08	1.8	1.2	34 ± 3.4	(11)	−6.5 ± 0.19	0.33	0.83	(4)
	V:08/5.42	H203A	111 ± 4.6	(3)	−8.9 ± 0.17	1.4	1.0	108 ± 24	(5)	−6.2 ± 0.08	0.58	1.4	(3)
TM-6	VI:13/6.48	W252A	51 ± 4.3	(3)	−9.1 ± 0.06	0.78	0.53**	75 ± 6.2	(11)	−6.1 ± 0.11	0.71	1.8*	(5)
	VI:16/6.51	Y255A	47 ± 3.5	(3)	−8.9 ± 0.11	1.1	0.77	32 ± 9.7	(7)	−6.6 ± 0.36	0.27	0.68	(5)
	VI:20/6.55	I259A	3.0 ± 0.3	(3)	−8.7 ± 0.09	2.1	1.4	59 ± 4.6	(7)	−7.1 ± 0.16	0.08	0.21***	(5)
	VI:20/6.55	I259W	34 ± 4.3	(3)	−8.9 ± 0.06	1.3	0.91	28 ± 4.2	(6)	−6.8 ± 0.20	0.15	0.38**	(5)
	VI:23/6.58	D262N[a]	54 ± 4.1	(3)	−8.2 ± 0.04	5.8	4.0***	63 ± 7.0	(23)	−5.2 ± 0.09	6.1	*15****	(11)
TM-7	VII:−02/7.32	H281A[a]	169 ± 29	(3)	−8.7 ± 0.13	1.8	1.2	33 ± 9.5	(18)	−6.1 ± 0.19	0.80	2.0*	(12)
	VII:02/7.35	I284A	56 ± 9.7	(4)	−8.6 ± 0.05	2.3	1.6*	38 ± 4.3	(13)	−6.6 ± 0.10	0.27	0.68	(5)
	VII:06/7.39	E288A[a]	77 ± 16	(5)	>−7	>100	**>68**	11 ± 4.0	(10)	Not determined			

Table 1

Continued

Receptor			[Cit¹]FC131				[Aib¹]FC131				[D-Arg¹]FC131			
Helix	Position	Mutation	EC_{50} ± SEM (log)	EC_{50} (μM)	F_{mut}	(*n*)	EC_{50} ± SEM (log)	EC_{50} (μM)	F_{mut}	(*n*)	EC_{50} ± SEM (log)	EC_{50} (μM)	F_{mut}	(*n*)
WT	WT	WT[a]	−5.5 ± 0.11	3.0	1.0	(22)	−5.5 ± 0.09	2.9	1.0	(24)	−6.3 ± 0.09	0.52	1.0	(19)
TM-1	I:07/1.39	Y45A	−4.8 ± 0.12	17	*5.7***	(4)	−4.3 ± 0.07	46	***16*****	(3)	−5.8 ± 0.10	1.6	3.0*	(4)
TM-2	II:20/2.60	W94A[a]	−6.8 ± 0.41	0.17	0.06***	(9)	−7.7 ± 0.14	0.02	0.01***	(3)	−7.3 ± 0.67	0.05	0.09**	(3)
	II:23/2.63	D97A[a]	−6.4 ± 0.02	0.44	0.15*	(3)	−6.5 ± 0.07	0.35	0.12**	(3)	−7.2 ± 0.05	0.06	0.12**	(3)
TM-3	III:05/3.29	H113A[a]	>−4	>100	***>33***	(10)	>−4	>100	***>35***	(5)	> −4	>100	**>170**	(3)
	III:08/3.32	Y116A[a]	Not determined				Not determined				Not determined			
	III:09/3.33	T117A	−5.4 ± 0.10	4.2	1.4	(3)	−6.0 ± 0.14	1.0	0.34	(3)	−6.1 ± 0.12	0.74	1.4	(3)
TM-4	IV:20/4.60	D171N[a]	−4.6 ± 0.12	25	*8.3****	(12)	−5.2 ± 0.18	6.2	2.2	(5)	−4.5 ± 0.27	28	**54*****	(4)
	ECL-2/Cys-3	R183A	Not determined				Not determined				Not determined			
ECL-2	ECL-2/Cys+1	D187A[a]	−6.1 ± 0.03	0.76	0.25	(3)	−6.3 ± 0.12	0.49	0.17**	(3)	−6.5 ± 0.15	0.35	0.66	(3)
	ECL-2/Cys+2	R188A	−4.4 ± 0.09	44	*15****	(3)	−5.0 ± 0.25	10	3.5	(3)	−5.7 ± 0.10	2.2	4.2*	(3)
	ECL-2/Cys+3	F189A	−6.1 ± 0.19	0.79	0.27*	(5)	−6.5 ± 0.30	0.31	0.11***	(6)	−6.8 ± 0.02	0.15	0.28*	(4)
	ECL-2/Cys+4	Y190A	−5.6 ± 0.54	2.6	0.87	(4)	−5.4 ± 0.13	4.0	1.4	(6)	−6.2 ± 0.24	0.66	1.3	(3)
TM-5	V:01/5.35	V196A	−5.4 ± 0.22	3.6	1.2	(3)	−5.3 ± 0.27	4.6	1.6	(3)	−5.8 ± 0.27	1.6	3.0	(3)
	V:04/5.38	F199A	−5.6 ± 0.17	2.3	0.77	(3)	−5.5 ± 0.06	2.9	1.0	(3)	−6.5 ± 0.16	0.31	0.59	(3)
	V:05/5.39	Q200A	−6.2 ± 0.12	0.61	0.20*	(3)	−5.2 ± 0.19	6.9	2.4	(3)	−6.2 ± 0.05	0.57	1.1	(3)
	V:05/5.39	Q200W	−5.6 ± 0.15	2.7	0.89	(3)	−5.5 ± 0.16	2.8	1.0	(4)	−6.1 ± 0.24	0.86	1.6	(3)
	V:08/5.42	H203A	−5.1 ± 0.24	8.0	2.7	(3)	−4.7 ± 0.12	20	*6.8***	(3)	−6.0 ± 0.15	0.98	1.9	(3)
TM-6	VI:13/6.48	W252A	−4.9 ± 0.19	13	4.3*	(5)	−4.8 ± 0.18	16	*5.8***	(5)	−5.5 ± 0.01	3.1	*6.0***	(3)
	VI:16/6.51	Y255A	−5.5 ± 0.24	3.2	1.1	(4)	−5.1 ± 0.30	8.5	3.0	(3)	−6.1 ± 0.55	0.8	1.6	(3)
	VI:20/6.55	I259A	−6.4 ± 0.49	0.41	0.14*	(3)	−6.3 ± 0.32	0.53	0.18*	(3)	−6.4 ± 0.53	0.4	0.84	(3)
	VI:20/6.55	I259W	−5.7 ± 0.23	2.2	0.74	(3)	−6.2 ± 0.19	0.68	0.24*	(3)	−6.2 ± 0.18	0.66	1.3	(3)
	VI:23/6.58	D262N[a]	−5.3 ± 0.13	5.5	1.8	(12)	−5.4 ± 0.13	4.3	1.5	(6)	−5.0 ± 0.18	10	***20*****	(4)
TM-7	VII:−02/7.32	H281A[a]	−5.3 ± 0.17	5.2	1.7	(7)	−6.4 ± 0.53	0.36	0.12**	(4)	−6.2 ± 0.29	0.60	1.1	(4)
	VII:02/7.35	I284A	−4.8 ± 0.42	15	4.9*	(3)	−5.4 ± 0.13	3.8	1.3	(4)	−5.6 ± 0.16	2.6	*5.0***	(4)
	VII:06/7.39	E288A[a]	Not determined				Not determined				Not determined			

IP turnover was measured in COS-7 cells co-transfected with CXCR4 receptor constructs and the promiscuous G-protein G_{qi4myr}. Residue positions are given according to the numbering systems of Baldwin/Schwartz and Ballesteros/Weinstein. The number of experiments is shown in parentheses, and F_{mut} indicates the fold-difference (ratio) between the potency on WT CXCR4 compared with mutant CXCR4 with codes as follows: bold >50; bold and italic >15, italic >5, underline <0.2. ***$P < 0.001$, **$P < 0.01$, *$P < 0.05$.

[a]Mutant also tested in binding assay (Table 2).

Table 2

Affinity of 12G5, FC131, [Cit[1]]FC131, [Aib[1]]FC131 and [D-Arg[1]]FC131 for WT CXCR4 and various CXCR4 mutations

Receptor			12G5						FC131				
Helix	Position	Mutation	IC_{50} ± SEM (log)	IC_{50} (nM)	F_{mut}	B_{max} ± SEM (fmol/10^5 cells)	(*n*)	*P* (B_{max})	IC_{50} ± SEM (log)	IC_{50} (μM)	F_{mut}	*P*	(*n*)
WT	WT	WT	−8.3 ± 0.13	4.7	1.0	0.096 ± 0.018	(12)		−6.1 ± 0.09	0.76	1.0		(12)
TM-2	II:20/2.60	W94A	−8.7 ± 0.15	1.9	0.40	0.053 ± 0.022	(8)		−7.5 ± 0.07	0.03	0.04	***	(9)
	II:23/2.63	D97A	−8.0 ± 0.12	9.4	2.0	0.086 ± 0.013	(3)		−6.8 ± 0.15	0.17	0.22	**	(3)
TM-3	III:05/3.29	H113A	−8.6 ± 0.15	2.7	0.58	0.037 ± 0.006	(7)	*	−4.3 ± 0.18	48	***63***	***	(8)
	III:08/3.32	Y116A	−8.1 ± 0.08	8.7	1.9	0.036 ± 0.016	(5)		> −4	>100	>**132**		(3)
TM-4	IV:20/4.60	D171N	−8.7 ± 0.18	2.2	0.47	0.034 ± 0.017	(7)	*	−4.3 ± 0.12	55	***72***	***	(8)
ECL-2	ECL-2 / Cys+1	D187A	−7.8 ± 0.04	16	3.4	0.161 ± 0.012	(3)		−5.1 ± 0.18	7.7	*10*	***	(3)
TM-6	VI:23/6.58	D262N	−8.4 ± 0.15	3.7	0.79	0.101 ± 0.020	(8)		−4.1 ± 0.18	73	***96***	***	(9)
TM-7	VII:−02/7.32	H281A	−8.6 ± 0.15	2.4	0.52	0.028 ± 0.008	(7)	*	−4.9 ± 0.11	13	*18*	***	(8)
	VII:06/7.39	E288A	−8.7 ± 0.16	2.1	0.45	0.035 ± 0.011	(7)	*	−5.4 ± 0.12	4.1	*5.5*	***	(8)

Receptor			[Cit[1]]FC131					[Aib[1]]FC131					[D-Arg[1]]FC131				
Helix	Position	Mutation	IC_{50} ± SEM (log)	IC_{50} (μM)	F_{mut}	*P*	(*n*)	IC_{50} ± SEM (log)	IC_{50} (μM)	F_{mut}	*P*	(*n*)	IC_{50} ± SEM (log)	IC_{50} (μM)	F_{mut}	*P*	(*n*)
WT	WT	WT	−5.3 ± 0.12	4.9	1.0		(11)	−5.5 ± 0.16	2.9	1.0		(5)	−6.4 ± 0.14	0.38	1.0		(6)
TM-2	II:20/2.60	W94A	−6.6 ± 0.16	0.27	0.06	***	(9)	−6.9 ± 0.33	0.14	0.05	**	(3)	−7.5 ± 0.09	0.03	0.08	**	(3)
	II:23/2.63	D97A	−6.1 ± 0.05	0.87	0.18	**	(3)	−5.9 ± 0.09	1.2	0.40	ns	(3)	**No displacement**				(3)
TM-3	III:05/3.29	H113A	>−4	>100	*>20*	***	(8)	**No displacement**				(3)	**No displacement**				(3)
	III:08/3.32	Y116A	>−4	>100	*>20*	***	(2)	**No displacement**				(2)	>−4	>100	**>261**		(3)
TM-4	IV:20/4.60	D171N	−4.3 ± 0.11	47	*9.6*	***	(8)	>−4	>100	>***34***	***	(3)	>−4	>100	**>261**		(3)
ECL-2	ECL-2 / Cys+1	D187A	−5.4 ± 0.20	4.3	0.87	ns	(3)	−5.6 ± 0.19	2.6	0.9	ns	(3)	−4.9 ± 0.17	12	***31***	***	(3)
TM-6	VI:23/6.58	D262N	−4.2 ± 0.10	61	*12*	***	(9)	>−4	>100	>***34***	***	(3)	>−4	>100	**>261**		(3)
TM-7	VII:−02/7.32	H281A	−4.5 ± 0.17	31	*6.3*	***	(8)	−4.0 ± 0.10	91	***31***	***	(3)	−4.0 ± 0.21	107	**280**	***	(3)
	VII:06/7.39	E288A	−5.7 ± 0.19	2.1	0.44	ns	(6)	−5.4 ± 0.10	4.2	1.4	ns	(3)	>−4	>100	**>261**		(3)

The data were obtained from competition binding with ^{125}I-labelled antibody 12G5 as radioligand on transiently transfected COS-7 cells. Values in parentheses represent number of experiments (*n*), and F_{mut} indicates the fold-difference (ratio) between the affinities on mutant receptor compared with WT receptor with codes as follows: bold >100 or no displacement at all, bold and italic >25, italic >5, underline <0.2. ***$P < 0.001$, **$P < 0.01$, *$P < 0.05$. Residue nomenclature is given in Table 1.

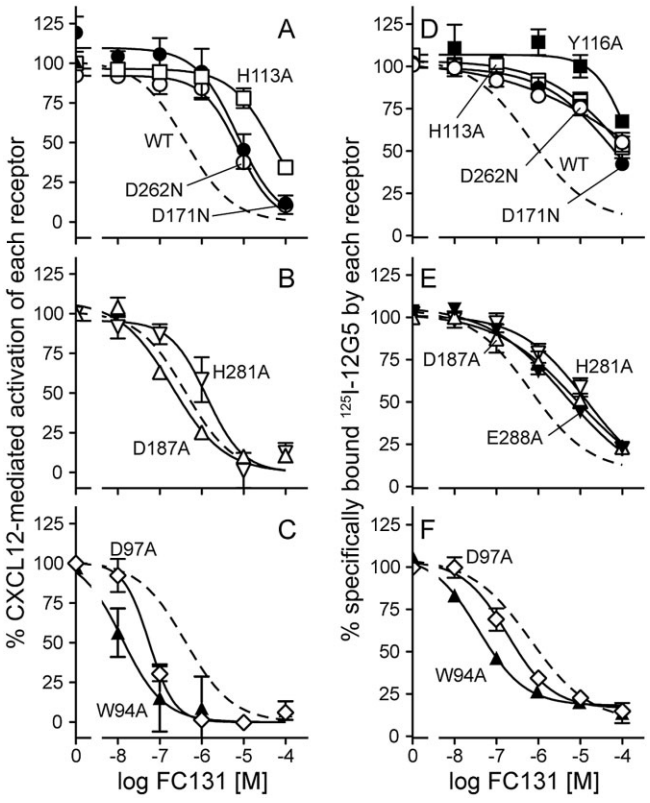

Figure 2

Mutational analysis of FC131 in CXCL12 inhibition and ^{125}I-12G5-binding studies. The ability of FC131 to inhibit CXCL12-mediated activation (A–C) or to displace ^{125}I-12G5 (D–F) from WT CXCR4 (stippled line) or mutants in the TM area (H113A, Y116A, D171N, D262N) (A and D), the exterior receptor parts (H281A, D187A) and E288A (B and E), or the minor binding pocket (W94A, D97A) (C and F) was assessed (see Methods for details). Y116A and E288A were not activated by CXCL12 and could therefore not be assessed in functional studies of FC131 (A and B); $n \geq 3$.

(Figure 2A), while no effects were observed for mutations in ECL-2 (D187A) and the top of TM-7 (H281A) (Figure 2B). Ala substitution of TM-2 residues Trp^{94} and Asp^{97}, pointing towards the minor binding pocket (defined by TM-1, -2, -3, -7), improved the potency of FC131 (Figure 2C). CXCL12-induced activity was highly impaired in Y116A and E288A, both pointing into the major binding pocket (delimited by TM-3 to -7, Figure 1C), and FC131 was consequently not tested further here. A large number of mutations in TM-3 (Thr^{117}), ECL-2 (Arg^{183}, Arg^{188}, Phe^{189}, Tyr^{190}), TM-5 (Val^{196}, Phe^{199}, Gln^{200}, His^{203}), TM-6 (Trp^{252}, Tyr^{255}, Ile^{259}) and TM-7 (Ile^{284}) did not impair the antagonistic potency of FC131 (Table 1). However, a small decrease (4.1-fold) was observed for Ala substitution of Tyr^{45} in TM-1.

The binding site of FC131 is located in the major binding pocket of CXCR4

The effect of the nine selected mutations on the affinity of FC131 was assessed in the ^{125}I-12G5 heterologous competition binding assay (Table 2). Here, similar results were obtained, yet with the expected generally larger changes in affinity (Table 2) as compared with changes in potency (Table 1). Thus, FC131 displayed high affinity to WT CXCR4 (IC_{50} of 0.74 μM), whereas the H113A, Y116A, D171N and D262N mutants resulted in 63- to >132-fold decreased affinities (Figure 2D). H281A and D187A resulted in a lower though significant decrease (18- and 10-fold respectively). A minor decrease in affinity was also observed for E288A (5.5-fold) (Figure 2E). Finally, in analogy to the functional assay results, W94A and D97A led to 25- and 4.6-fold *increased* affinities respectively (Figure 2F).

Molecular docking of FC131 in CXCR4

Next, FC131 was docked to the X-ray crystal structure of CXCR4 [PDB code 3OE0 (Wu *et al.*, 2010)] using the induced-fit docking protocol developed by Schrödinger (see Methods). As the binding and functional studies (Tables 1 and 2) both showed a dependence on the spatially close residues His^{113} (TM-3) and Asp^{171} (TM-4), a H-bond constraint was set on the carboxylate group of Asp^{171}. The following binding mode, which was among the top 10 optimized poses and supports the experimental data outlined above, is suggested (Figure 3A–C): Arg^{1} of FC131 interacts with Asp^{187} while Arg^{2} interacts with His^{113}/Asp^{171}; although also a direct interaction of Asp^{97} with Arg^{1} in FC131 is observed in this docking pose (not shown) and in earlier computational studies (Demmer *et al.*, 2011; Mungalpara *et al.*, 2012; Yoshikawa *et al.*, 2012), the observation that the D97A mutation led to an increased affinity and potency of FC131 argues for a different role of Asp^{97} (Figure 2C and F). The aromatic 2-Nal^{3} side chain is positioned in a tight hydrophobic pocket facing TM-5, and sandwiched between Arg^{188} (cation-π interactions) and His^{203} (π-π interactions). In most poses, D-Tyr^{5} of FC131 points towards Glu^{32} in the receptor N-terminus, while in some poses an interaction with Asp^{262} was observed (not shown). Finally, Glu^{288} interacts with the backbone of the ligand via a water-mediated H-bond network. Thus, FC131 binds in the major binding pocket of CXCR4, with the Arg^{2} and 2-Nal^{3} side chains buried deeply, while the Arg^{1} and D-Tyr^{5} side chains point outwards.

Overall, His^{113}, Asp^{171}, Asp^{187} and Glu^{288} are part of the binding site (Glu^{288} via water molecules), confirming recently suggested binding modes for FC131 (Demmer *et al.*, 2011; Mungalpara *et al.*, 2012; Yoshikawa *et al.*, 2012), while Tyr^{45}, Tyr^{116} and His^{281} do not directly interact with FC131, but nevertheless influence its binding and activity to varying extents. A direct interaction of D-Tyr^{5} of FC131 with Asp^{262} is only seen in a few poses and is not likely to account for the large effect of the D262N mutation (96- and 12-fold decrease in affinity and potency, respectively, of FC131). However, Asp^{262} is a central residue in a H-bond network involving Gln^{200} (TM-5), His^{281} (TM-7), and Arg^{30} (N-terminus) (not shown), and removal of the charge in Asp^{262} may disturb this network and thereby indirectly affect FC131 binding and function.

[Cit^{1}]FC131 without a positively charged side chain in position 1 loses dependency on Asp^{187} in ECL-2

Previous SAR studies of FC131 (Figure 4A) have shown that Arg^{1} (but not Arg^{2}) can be replaced with the uncharged L-Cit

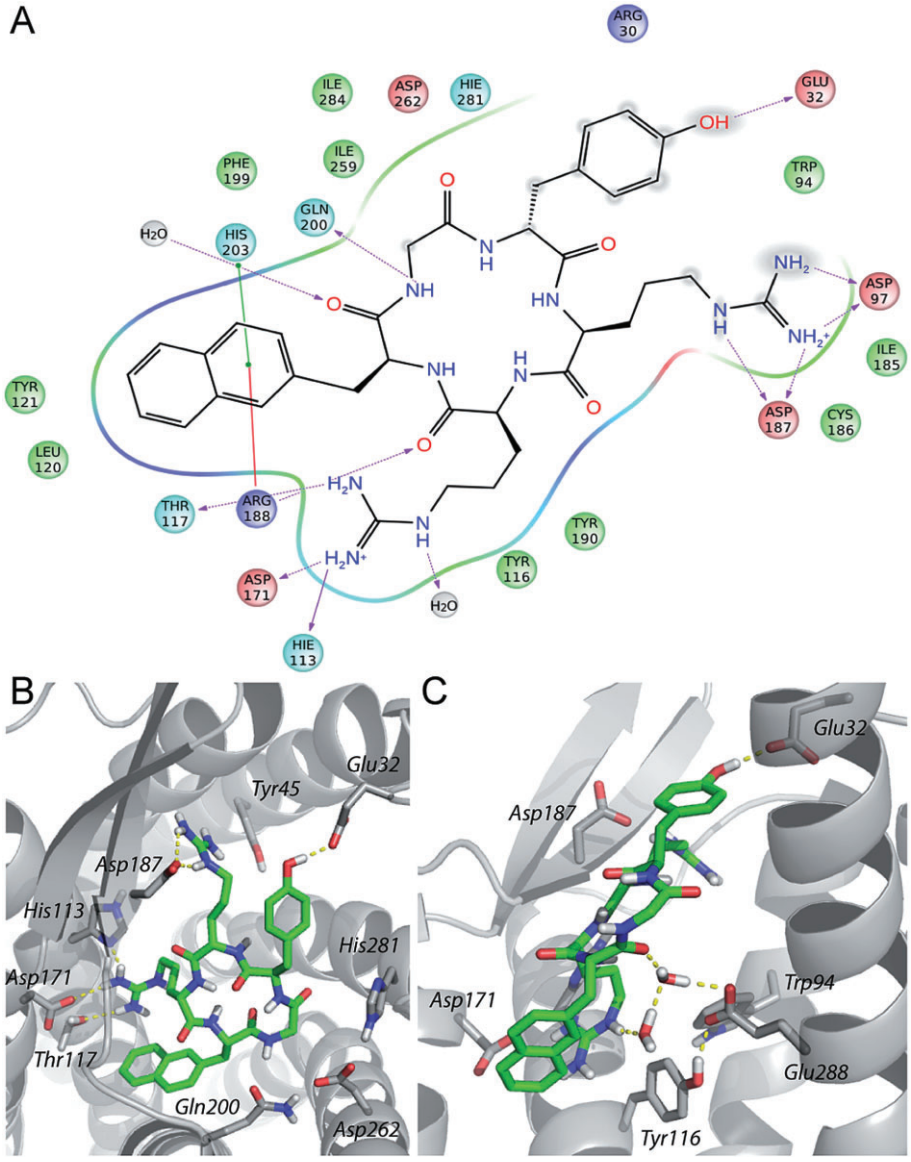

Figure 3

The binding mode of FC131 in CXCR4. (A) Two-dimensional representation of the FC131-binding site in CXCR4. Residue colours: red, negative; purple, positive; cyan, polar; green, hydrophobic. Interactions: pink full and stippled arrows, H-bond with main and side chain respectively; green line, π-π stacking; red line, cation-π interaction; grey cloud, solvent-exposed atom. Three-dimensional model of FC131 binding in CXCR4 as seen from top (B) or the side (C). TM-5 and -6 have been removed for clarity.

residue (Figure 4B) (Mungalpara *et al.*, 2012). In order to confirm the suggested binding mode of FC131 (Figure 3), we subjected the [Cit[1]]FC131 analogue to the same mutational analysis in ^{125}I-12G5-binding and CXCL12-functional studies. Consistent with previous data (Mungalpara *et al.*, 2012), [Cit[1]]FC131 displayed six- to eightfold lower affinity and potency as compared with FC131 (Tables 1 and 2). However, the effect of most mutations on [Cit[1]]FC131 was similar to that observed for FC131 (Figure 4D). Thus, mutation of residues facing the major binding pocket (H113A, Y116A, D171N, D262N) resulted in 9.6- to >20-fold decreases in affinity (Figure 4E and Table 2). H281A, in the top of TM-7, led to a 6.3-fold decrease, while E288A resulted in a partial displacement with unchanged affinity. Furthermore, as for FC131, mutations in TM-2 of the minor binding pocket (W94A and D97A) led to increased affinities (Table 2). However, contrary to what was observed for FC131 (Figure 4D), D187A in ECL-2 did not affect the binding of [Cit[1]]FC131 (Figure 4E). Thus, the affinity of FC131 on D187A (IC_{50} of 7.7 μM) is similar to the affinity of [Cit[1]]FC131 on WT CXCR4 (IC_{50} of 4.9 μM), pointing towards an interaction of side chain 1 with Asp[187].

The effect of receptor mutants on the ability of [Cit[1]]FC131 to inhibit CXCL12-mediated activation confirmed the picture observed in ^{125}I-12G5 binding. Mutation of residues in the major binding pocket, including those located deeply and those located more superficially, resulted in

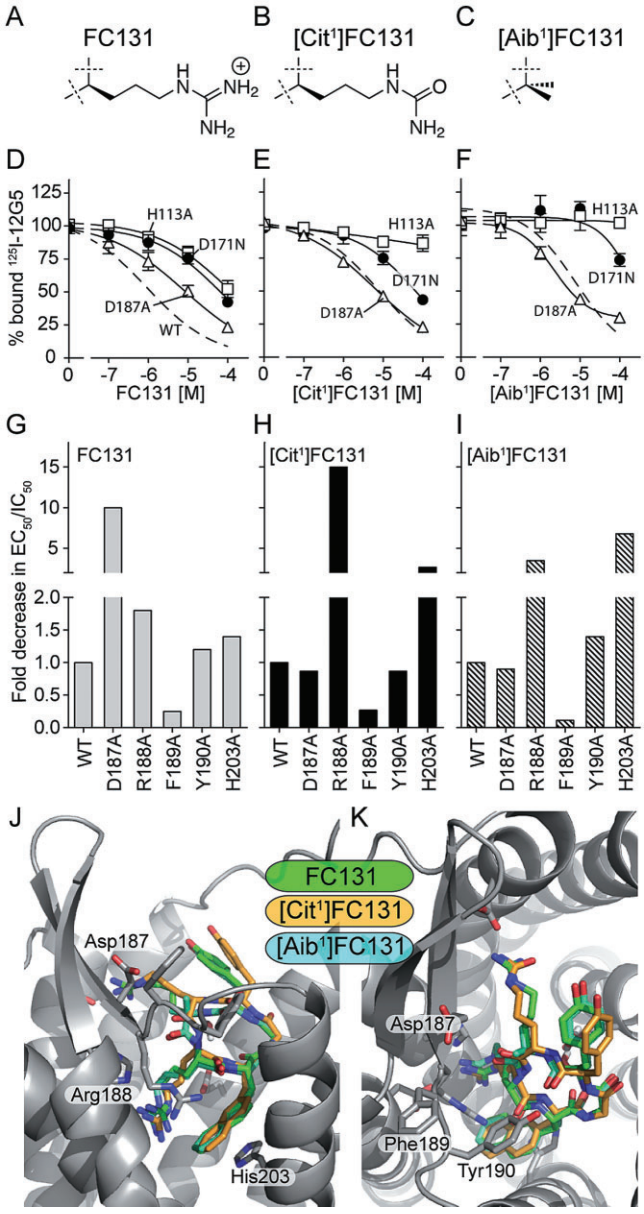

Figure 4

[Cit¹]FC131 and [Aib¹]FC131 confirm the orientation of FC131 in CXCR4, and highlight the role of Arg^{188} and His^{203} for sandwiching the 2-Nal^{3} side chain. The structures of the side chains in position 1 of FC131 (A), [Cit¹]FC131 (B) and [Aib¹]FC131 (C) are given. (D–F) ^{125}I-12G5-binding assays on WT CXCR4 and mutant receptors (H113A, D171N and D187N, symbols as in Figure 2). (G–I) Effects of mutations D187A, R188A, F189A, Y190A (ECL-2) and H203A (TM-5) in binding (D187A) or functional assays (other mutants) shown as fold decreases. (J and K) Molecular docking of the analogues.

strongly (H113A) or moderately (I284A, D171N) decreased or unchanged (D262N, H281A) potency of [Cit¹]FC131 (Table 1). The lack of effect for D262N could be due to the generally smaller dynamic window in functional studies compared with ^{125}I-12G5 binding and the smaller effect observed in binding for [Cit¹]FC131 (12-fold) versus FC131 (96-fold). Furthermore, the potency of [Cit¹]FC131 was decreased 5.7-fold for Y45A, while mutation of residues in TM-2 led to increased potencies (W94A, D97A) (Table 1). As expected from ^{125}I-12G5-binding experiments, D187A did not impair the antagonistic potency of [Cit¹]FC131 (Figure 4H). Analysis of neighbouring residues in ECL-2 (Figure 4G and H) revealed that Ala substitution of Arg^{188} led to a 15-fold reduced potency of [Cit¹]FC131 (Figure 4H), while having no effect on FC131 (Figure 4G). None of the other aromatic residues in ECL-2 (Phe^{189}, Tyr^{190}) affected the potency of either [Cit¹]FC131 or FC131 (Figure 4G and H). This highlights the effect of the cation-π interaction between 2-Nal^{3} and Arg^{188} in the absence of Arg^{1}. Molecular docking of [Cit¹]FC131 into CXCR4 also reveals that Asp^{187} is pointing away from side chain Cit^{1} (Figure 4J and K). Of the remaining mutations (Thr^{117}, Val^{196}, Phe^{199}, Gln^{200}, His^{203}, Trp^{252}, Tyr^{255}, Ile^{259}), only W252A led to 4.3-fold impaired potency (Table 1).

[Aib¹]FC131, which lacks a side chain functionality in position 1, displays the same binding mode as FC131 and [Cit¹]FC131

As described above, FC131 tolerates removal of the positive charge from the side chain in position 1. It also tolerates truncation of this side chain to the backbone stabilizing disubstituted residue Aib, that is, [Aib¹]FC131 (Figure 4C) (Mungalpara *et al.*, 2012), which has the same affinity and potency as [Cit¹]FC131 (Tables 1 and 2). The mutagenesis study of this compound in ^{125}I-12G5 binding revealed a stronger dependence on residues in the major binding pocket (H113, Y116, D171, D262, H281) than for [Cit¹]FC131. However, in analogy with [Cit¹]FC131, no effect was observed for D187A or E288A, while W94A and D97A led to similar increases in affinity (Table 2, Figure 4F). [Aib¹]FC131 also mirrored [Cit¹]FC131 in the functional studies with a few exceptions (Table 1): compared with [Cit¹]FC131 it showed decreased dependency on Asp^{171} and Arg^{188} in TM-IV and ECL-2 respectively. In contrast, it depended to a higher degree on His^{203}, as its potency was decreased 6.8-fold by H203A (Figure 4I), while that of [Cit¹]FC131 was only impaired 2.7-fold (Figure 4H). Thus, the importance of Arg^{188} and His^{203} in sandwiching the 2-Nal^{3} side chain, as discussed above, seems to change from Arg^{188} for [Cit¹]FC131 to His^{203} for [Aib¹]FC131. Furthermore, Y45A resulted in 16-fold decreased potency of [Aib¹]FC131, compared with the smaller impact of 5.7-fold for [Cit¹]FC131. Finally, computational modelling confirms a binding mode that overlaps with those of FC131 and [Cit¹]FC131 for side chains L-Arg^{2}, 2-Nal^{3}, Gly^{4} and D-Tyr^{5} (Figure 4J and K). This emphasizes that side chain 1 is not required for achieving this binding mode of cyclopentapeptides in CXCR4, yet plays a role for high potency and affinity, as described earlier (Tamamura *et al.*, 2005a; Demmer *et al.*, 2011; Mungalpara *et al.*, 2012).

The close analogue [D-Arg¹]FC131 behaves differently than FC131 in its ability to displace ^{125}I-12G5

[D-Arg¹]FC131 differs from FC131 only in the stereochemistry in position 1 and displays similar potency and two-fold higher affinity; however, this compound interacted differently with CXCR4. In ^{125}I-12G5-binding experiments, a stronger dependency was observed on His^{113}, Tyr^{116}, Asp^{171},

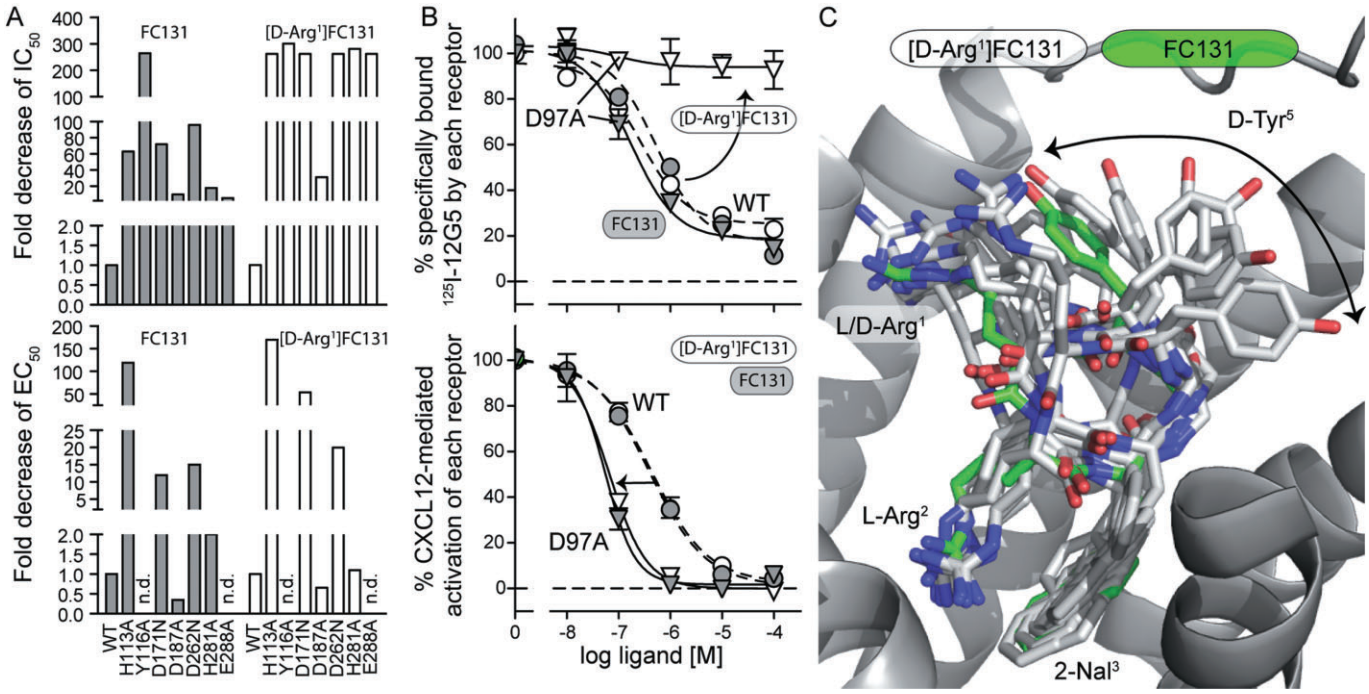

Figure 5

Mutational analysis and computational modelling of [D-Arg^1]FC131 binding in CXCR4. (A) Fold decreases of FC131 and [D-Arg^1]FC131 affinity (upper diagram) and antagonistic potency (lower diagram) observed for a range of mutants in comparison to WT CXCR4. (B) The effect of D97A in comparison to WT (stippled line) on the affinity (upper part) and potency (lower part) of FC131 and [D-Arg^1]FC131. (C) Molecular docking of [D-Arg^1]FC131 (white structures) showing multiple binding poses in overlay with the FC131-binding pose (green structure). n.d., not determined.

Asp^{187}, Asp^{262}, His^{281} and Glu^{288} for [D-Arg^1]FC131 than for FC131, while in functional assays both compounds behaved largely similar on all mutants (Figure 5A, Tables 1 and 2). Interestingly, [D-Arg^1]FC131 acted differently on mutations in TM-2 than FC131; while W94A consistently led to increased affinities and potencies, D97A abrogated the ability of [D-Arg^1]FC131 to displace ^{125}I-12G5, while it, as for FC131, increased its antagonistic potency (Figure 5B). Molecular docking of [D-Arg^1]FC131 to CXCR4 revealed a larger flexibility of the exteriorly located part of the molecule as compared with FC131. While D-Arg^1 still mainly interacted with Asp^{187}, D-Tyr^5 displayed a larger degree of conformational freedom and pointed everywhere from TM-2 and the N-terminus to TM-6 (Figure 5C); however, the crucial ligand side chains Arg^2 and 2-Nal^3 bound to His^{113}/Asp^{171} and the hydrophobic pocket around TM-5 in the same way as in FC131.

A H-bond between Tyr^{116} and Glu^{288} plays a role in the activation of CXCR4

In the crystal structure of the complex between CXCR4 and the peptide antagonist CVX15 (Figure 6A) (Wu *et al.*, 2010) and in our models of the receptor-bound cyclopentapeptide ligands (Figure 3C), a H-bond is observed between Tyr^{116} in TM-3 and Glu^{288} in TM-7. *In vitro* experiments showed that Ala substitution of Tyr^{116} or Glu^{288} abolished the agonistic action of CXCL12 (Figure 6B), despite surface expression levels of 69 and 77% of WT respectively (Table 1). Both mutant receptors bound ^{125}I-12G5 with WT-like affinities, suggesting proper folding of the receptors (Figure 6C). Furthermore, all four cyclopentapeptide ligands were unable to displace ^{125}I-12G5 from Y116A-CXCR4, while only [D-Arg^1]FC131 was affected by E288A (Figure 6D, Table 2). Although Tyr^{116} was not revealed as a direct interaction partner for the cyclopentapeptide ligands in the docking studies, these mutagenesis data point towards a role of Tyr^{116} for the ability of the ligands to displace ^{125}I-12G5. Furthermore, the H-bond between Tyr^{116} and Glu^{288} seems crucial for the activation of CXCR4 by CXCL12. Further studies are needed to fully understand the functional importance of the link between Tyr^{116} and Glu^{288} in CXCR4.

Discussion and conclusions

We have used a dual approach combining receptor mutational analysis with ligand modifications to determine the binding mode of FC131 in CXCR4: Arg^1, Arg^2, 2-Nal^3 and D-Tyr^5 of FC131 interact with ECL-2 (Asp^{187}), TM-3/-4 (His^{113}, Asp^{171}), TM-5 and the exterior receptor part (Glu^{32}) respectively. The orientation of FC131 in the pocket was confirmed by [Cit^1]FC131 and [Aib^1]FC131 that both lack the positive charge at position 1 and at the same time do not depend on Asp^{187}. Overall, our data are consistent with earlier proposed binding modes predicting Arg^1 and D-Tyr^5 to point outwards, while Arg^2 and 2-Nal^3 interact with residues deep in the major binding pocket (Figure 3) (Demmer *et al.*, 2011; Yoshikawa *et al.*, 2012; Mungalpara *et al.*, 2013).

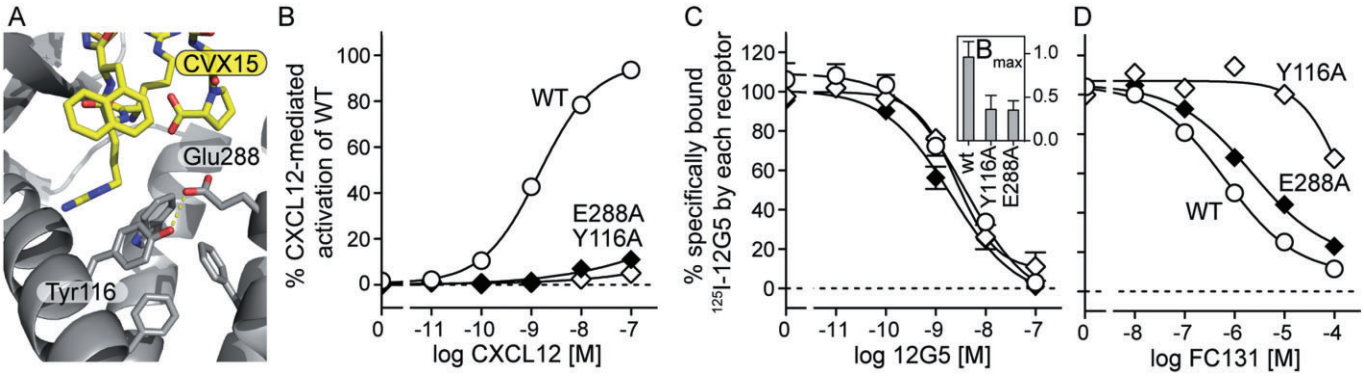

Figure 6

Mutation of the H-bond forming residues Tyr[116] and Glu[288] abolished CXCL12-induced receptor activation. (A) Tyr[116] and Glu[288] form a H-bond in the crystal structure of CXCR4 (here bound to CVX15, PDB code 3OE0). (B) Ability of CXCL12 to activate WT CXCR4 and mutants Y116A and E288A. (C) Homologous ^{125}I-12G5-competition binding experiments on WT, Y116A and E288A (symbols as in A) and the B_{max} of 12G5 in fmol/10^6 cells for each receptor (inset). (D) Ability of FC131 to displace ^{125}I-12G5 from WT, Y116A and E288A (symbols as in A).

Comparison of the binding modes of FC131, CVX15 and AMD compounds

The recent crystal structure of CXCR4 with the low MW compound IT1t or the peptide CVX15 (Wu *et al.*, 2010) gave first-hand insights into antagonist interaction with CXCR4. Surprisingly, IT1t interacted with residues Glu[288], Asp[187] and Asp[97] in the *minor binding pocket*, while the peptide ligand CVX15, a 16-mer analogue of the 14-mer T140 that FC131 was developed from, was located in the *major binding pocket* and in extracellular receptor regions. Specifically, Arg[1] of CVX15 interacted with Asp[187], Arg[2] with His[113]/Asp[171], and Arg[14] with Asp[262] (Wu *et al.*, 2010). We find that FC131 mimics the binding of CVX15 as it interacts with Asp[187] via Arg[1], and His[113]/Asp[171] via Arg[2]. Thus, the two arginine residues in FC131 correspond to Arg[1] and Arg[2] of CVX15, and not to Arg[2] and Arg[14] as originally intended (Figure 7). Asp[262] was not found to interact with Arg[1] or Arg[2] of FC131 in any docking pose. Alternatively, the effect of D262N might be attributed to a central role of this residue in a H-bond network involving Arg[30], Gln[200] and His[281], as mentioned above. Furthermore, a link between ECL-2 (carrying Asp[187]) and Asp[262] is established via Gln[200] in TM-5, which is directly linked to ECL-2. Removing a conformational constraint between Asp[262] in TM-6 and Gln[200] in TM-5 might therefore alter the position of ECL-2. Such a scenario would also explain the weakened effect of D262N on analogues [Cit[1]]FC131 and [Aib[1]]FC131, lacking the positive charge at position 1 and dependency on Asp[187] in ECL-2.

Finally, 2-Nal[3] of FC131 and the corresponding 1-Nal[3] of CVX15 bind in a hydrophobic sub-pocket at TM-5; however, as previously suggested by comparing SAR data for the cyclopentapeptides and the larger peptide antagonists, the naphthyl groups do not completely overlap (Mungalpara *et al.*, 2013). Clearly, the 2-Nal[3] side chain of FC131 goes deeper into the hydrophobic sub-pocket, and presumably contributes more to activity than the 1-Nal[3] side chain of CVX15. The tyrosine residue in position 5 of both ligands takes up different positions. While Tyr[5] of CVX15 faces the upper part of the hydrophobic pocket around TM-5 (Wu *et al.*, 2010), rotation of D-Tyr[5] to Glu[32] (N-terminus) was observed in the

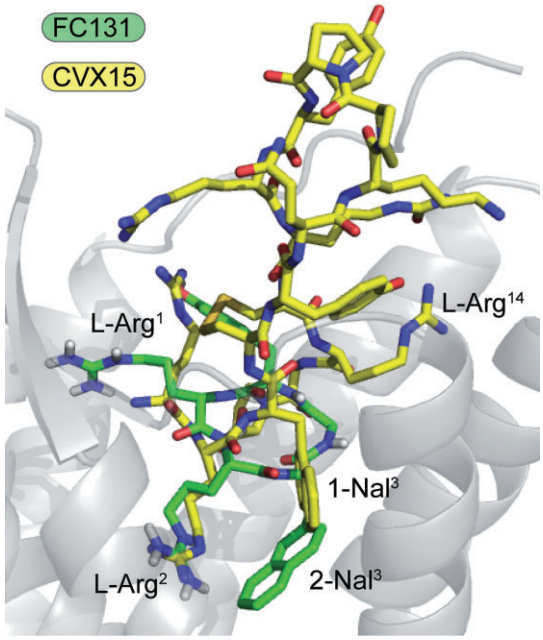

Figure 7

The binding of FC131 compared with CVX15. Overlay of the binding modes for FC131 (green) identified in the present study and CVX15 (yellow) from the co-crystal structure of CXCR4 and CVX15 (PDB code: 3OE0).

FC131-CXCR4 complex, again in agreement with SAR studies on this position suggesting a solvent-exposed, freely rotatable position in CXCR4 (Mungalpara *et al.*, 2013).

The well-described non-peptide AMD-compound series (the bicyclam AMD3100, the monocyclam AMD3465 and the non-cyclam AMD11070) was earlier shown to depend on Asp[262]/Glu[288] in TM-6/-7 on one side, and Asp[171] in TM-4 on the opposite side of the major binding pocket (Gerlach *et al.*, 2003; Rosenkilde *et al.*, 2004; 2007). Furthermore, mutation of residues in the minor binding pocket was found to impair

their action and multiple binding modes were subsequently suggested (Gerlach *et al.*, 2003; Rosenkilde *et al.*, 2004; 2007; Hatse *et al.*, 2005; Wong *et al.*, 2008; Gudmundsson *et al.*, 2009a,b; Catalano *et al.*, 2010; Miller *et al.*, 2010; Skerlj *et al.*, 2011). In the present study, FC131 was found to only indirectly interact with Glu^{288} via a water-mediated H-bond network, and therefore behaves somewhat differently from these reference CXCR4 antagonists and from most other small-molecule antagonists where the chemokine receptor-conserved Glu in position VII:06/7.39 seems to function as a general anchor point for positively charged nitrogens (Rosenkilde and Schwartz, 2006).

The role of ECL-2 in the binding of cyclic pentapeptides in CXCR4

ECL-2 connects TM-4 with TM-5 and is covalently linked to the top of TM-3 via a conserved disulphide bond. Thereby, the C-terminal part of ECL-2 (also called ECL-2b) is being held close to the extracellular surface of the main binding crevice of CXCR4. Asp^{187} is located in position Cys+1 in ECL-2b and the D187A mutation resulted in decreased affinities of FC131, but not [Cit^1]FC131, pointing towards an interaction of Asp^{187} with Arg^1 of the cyclopentapeptides. The adjacent Arg^{188} was earlier suggested to interact with the aromatic 2-Nal^3 side chain of FC131 by engaging in a cation-π interaction. This is also observed in our studies (Figure 4H), yet we do not see an effect of R188A on the potency of FC131, whereas the potency of [Cit^1]FC131 decreases by 15-fold and that of [Aib^1]FC131 by 3.5-fold (however, for [Aib^1]FC131 a role of the second suggested interaction partner for 2-Nal^3, His^{203} in TM-V, becomes visible) (Table 1). Thus, Asp^{187} seems to be the most important residue for FC131 in ECL-2, yet in the absence of the interaction between Arg^1 in FC131 and Asp^{187} (in [Cit^1] and [Aib^1]FC131), the impact of Arg^{188} becomes visible. Alternatively, Arg^{188} of CXCR4 and Arg^1 of FC131 might repel each other. Thus, the R188A mutation would remove the favourable interaction with 2-Nal^3, but also the unfavourable electrostatic repulsion of Arg^1, leading to a zero net effect of R188A on FC131. Importantly, a similar direct role of ECL-2b was found for the CCR5 antagonist aplaviroc (Maeda *et al.*, 2006; Thiele *et al.*, 2011). In a broader perspective, binding of small-molecule compounds to extracellular chemokine receptor domains has the potential of overlapping with the binding sites of chemokines, which due to their large size interact with the exterior parts of their receptors (Allen *et al.*, 2007; Scholten *et al.*, 2012). Low MW antagonists, although by default considered allosteric, may therefore become partially overlapping, resulting in competitive behaviour.

The role of Tyr^{116} for the function of CXCR4 antagonists

According to the two-step model of chemokine receptor activation, the interaction between CXCR4 and CXCL12 involves distinct receptor and chemokine domains in binding and activation (Crump *et al.*, 1997; Gupta *et al.*, 2001). In CXCR4, the initial high-affinity binding is mainly mediated by sulpho-tyrosines in the receptor N-terminus that interact with positively charged residues of CXCL12. In a second step, N-terminal CXCL12 residues interact with transmembrane receptor residues, and presumably also ECL-2 to induce receptor activation (Crump *et al.*, 1997; Ludeman and Stone, 2013). In agreement with this model, and consistent with the data presented here, Ala substitution of transmembrane residues Asp^{97}, Tyr^{116} and Glu^{288} affects the signalling properties (Table 1, Figure 6), but not the binding, of CXCL12 (Rosenkilde *et al.*, 2007; Wong *et al.*, 2008). Thus, it can be speculated that the observed H-bond between Tyr^{116} and Glu^{288} (Wu *et al.*, 2010) is crucial for CXCL12-mediated receptor activation. Furthermore, the function of all tested cyclopentapeptides depended on Tyr^{116} (Table 2, Figure 6D), probably via an indirect mechanism, as no direct interaction with the ligand was observed (Figure 3C). Interestingly, the function of AMD3100 and AMD3465 has also been shown to depend on Tyr^{116} (Wong *et al.*, 2008); however, it remains to be determined whether this effect is direct or indirect. Finally, as described above, Glu^{288} was found to be an indirect interaction partner for FC131, but mutation only resulted in minor effects for most cyclopentapeptide ligands, except binding of [D-Arg^1]FC131 (Table 2). Thus, the Tyr^{116}-Glu^{288} H-bond at the bottom of the major binding pocket is central not only for the activation but also for the inhibition of CXCR4, and consequently for the activity states of CXCR4.

The entrance to the binding crevice in CXCR4 is covered by H-bond and Cys bridge

While mutations in TM-2 (W94A, D97N) impair the affinity of the AMD compounds (Wong *et al.*, 2008), we observed that W94A and D97A increased the potencies and affinities of the cyclopentapeptide antagonists. In the crystal structure of CXCR4, Asp^{97} forms a salt bridge with Arg^{183} in ECL-2, which together with the chemokine receptor-conserved disulphide bridge between the N-terminus and top of TM-7 results in a partly covered major binding pocket (Wu *et al.*, 2010). This is not seen in the newly released structure of CCR5, which lacks Asp^{97} (or an equivalent thereof) and has a more open entrance to its binding pocket (Tan *et al.*, 2013). Although speculative, it could therefore be argued that breaking the Asp^{97}/Arg^{183}-salt bridge by Ala substitution of Asp^{97} releases the closed extracellular conformation of CXCR4 and gives FC131 easier access to its binding pocket. Mutation R183A does however not lead to increased potency of FC131 (Table 1); yet in the absence of the Arg^{183} side chain, it can be speculated that another residue takes over its function in the salt bridge to Asp^{97}; a H-bond is indeed observed between Asp^{97} and the backbone of Cys^{186}. W94A may have a similar effect by providing more space for Asp^{97}, thereby breaking the H-bond with Arg^{183}, or simply by creating more room for the ligand.

In conclusion, by combining receptor mutagenesis with ligand modifications, we determined the binding site of FC131 in CXCR4. In addition, our studies suggest a H-bond in the centre of the receptor between Tyr^{116} and Glu^{288} to be essential for the activation state of CXCR4. Finally, consistent with other studies of class A 7TM receptors, such as EBI2 (GPR183), CCR5 and CCR2, where a central role of the top of TM-2 is identified for the activity state (Alvarez Arias *et al.*, 2003; Benned-Jensen and Rosenkilde, 2008; Rosenkilde *et al.*, 2010), a possible gating function of the top of TM-2 for the entrance into the main binding crevice of CXCR4 is suggested, implying that improved CXCR4 antagonists could be

obtained by creating smaller molecules that can easily migrate into the main binding crevice of CXCR4.

Acknowledgements

Financial support for this project was obtained from the Research Council of Norway (Grant 190728/V30) (J. M. and J. V.) and from the Danish Council for Independent Research/ Medical Sciences, the NovoNordisk Foundation, the Lundbeck Foundation and the European Community's Sixth Framework Program (INNOCHEM: Grant LSHBCT-2005-518167) (S. T., A. S. and M. M. R). We also thank Inger Smith Simonsen, Randi Thøgersen and Maibritt Sigvardt Baggesen for outstanding technical assistance with the biological assays.

Author contributions

J. V., M. M. R. and S. T.: Experimental design. J. M.: Compound synthesis. S. T.: Binding studies. S. T., A. S. and J. M.: Functional studies. S. T.: ELISA. S. T. and J. M.: Data analysis. J. M. and J. V.: Computational modelling. S. T., J. M., M. M. R. and J. V.: Manuscript writing.

Conflict of interest

None.

References

Alexander SPH, Benson HE, Faccenda E, Pawson AJ, Sharman JL Spedding M *et al* (2013). The Concise Guide to PHARMACOLOGY 2013/14: G Protein-Coupled Receptors. Br J Pharmacol 170: 1459–1581.

Allen SJ, Crown SE, Handel TM (2007). Chemokine: receptor structure, interactions, and antagonism. Annu Rev Immunol 25: 787–820.

Alvarez Arias D, Navenot J-M, Zhang W-B, Broach J, Peiper SC (2003). Constitutive activation of CCR5 and CCR2 induced by conformational changes in the conserved TXP motif in transmembrane helix 2. J Biol Chem 278: 36513–36521.

Bachelerie F, Ben-Baruch A, Burkhardt AM, Combadiere C, Farber JM, Graham GJ *et al.* (2014). International union of basic and clinical pharmacology. LXXXIX. Update on the extended family of chemokine receptors and introducing a new nomenclature for atypical chemokine receptors. Pharmacol Rev 66: 1–79.

Baldwin JM, Schertler GF, Unger VM (1997). An alpha-carbon template for the transmembrane helices in the rhodopsin family of G-protein-coupled receptors. J Mol Biol 272: 144–164.

Balkwill F (2004). The significance of cancer cell expression of the chemokine receptor CXCR4. Semin Cancer Biol 14: 171–179.

Ballesteros JA, Weinstein H (1995) Integrated methods for the construction of three-dimensional models and computational probing of structure-function relations in G protein-coupled receptors. In: Sealfon SC (ed.). Receptor Molecular Biology. Academic Press: San Diego, CA, pp. 366–428.

Benned-Jensen T, Rosenkilde MM (2008). Structural motifs of importance for the constitutive activity of the orphan 7TM receptor EBI2: analysis of receptor activation in the absence of an agonist. Mol Pharmacol 74: 1008–1021.

Berson JF, Long D, Doranz BJ, Rucker J, Jirik FR, Doms RW (1996). A seven-transmembrane domain receptor involved in fusion and entry of T-cell-tropic human immunodeficiency virus type 1 strains. J Virol 70: 6288–6295.

Brandish PE, Hill LA, Zheng W, Scolnick EM (2003). Scintillation proximity assay of inositol phosphates in cell extracts: high-throughput measurement of G-protein-coupled receptor activation. Anal Biochem 313: 311–318.

Catalano JG, Gudmundsson KS, Svolto A, Boggs SD, Miller JF, Spaltenstein A *et al.* (2010). Synthesis of a novel tricyclic 1,2,3,4,4a,5,6,10b-octahydro-1,10-phenanthroline ring system and CXCR4 antagonists with potent activity against HIV-1. Bioorg Med Chem Lett 20: 2186–2190.

Choi W-T, Duggineni S, Xu Y, Huang Z, An J (2012). Drug discovery research targeting the CXC chemokine receptor 4 (CXCR4). J Med Chem 55: 977–994.

Crump MP, Gong JH, Loetscher P, Rajarathnam K, Amara A, Arenzana-Seisdedos F *et al.* (1997). Solution structure and basis for functional activity of stromal cell-derived factor-1; dissociation of CXCR4 activation from binding and inhibition of HIV-1. EMBO J 16: 6996–7007.

De Clercq E, Yamamoto N, Pauwels R, Balzarini J, Witvrouw M, De Vreese K *et al.* (1994). Highly potent and selective inhibition of human immunodeficiency virus by the bicyclam derivative JM3100. Antimicrob Agents Chemother 38: 668–674.

Demmer O, Dijkgraaf I, Schumacher U, Marinelli L, Cosconati S, Gourni E *et al.* (2011). Design, synthesis, and functionalization of dimeric peptides targeting chemokine receptor CXCR4. J Med Chem 54: 7648–7662.

DiPersio JF, Micallef IN, Stiff PJ, Bolwell BJ, Maziarz RT, Jacobsen E *et al.* (2009a). Phase III prospective randomized double-blind placebo-controlled trial of plerixafor plus granulocyte colony-stimulating factor compared with placebo plus granulocyte colony-stimulating factor for autologous stem-cell mobilization and transplantation for patients with non-Hodgkin's lymphoma. J Clin Oncol 27: 4767–4773.

DiPersio JF, Stadtmauer EA, Nademanee A, Micallef INM, Stiff PJ, Kaufman JL *et al.* (2009b). Plerixafor and G-CSF versus placebo and G-CSF to mobilize hematopoietic stem cells for autologous stem cell transplantation in patients with multiple myeloma. Blood 113: 5720–5726.

Feng Y, Broder CC, Kennedy PE, Berger EA (1996). HIV-1 entry cofactor: functional cDNA cloning of a seven-transmembrane, G protein-coupled receptor. Science 272: 872–877.

Fujii N, Oishi S, Hiramatsu K, Araki T, Ueda S, Tamamura H *et al.* (2003). Molecular-size reduction of a potent CXCR4-chemokine antagonist using orthogonal combination of conformation- and sequence-based libraries. Angew Chem Int Ed Engl 42: 3251–3253.

Gerlach LO, Jakobsen JS, Jensen KP, Rosenkilde MR, Skerlj RT, Ryde U *et al.* (2003). Metal ion enhanced binding of AMD3100 to Asp262 in the CXCR4 receptor. Biochemistry 42: 710–717.

Gudmundsson KS, Boggs SD, Catalano JG, Svolto A, Spaltenstein A, Thomson M *et al.* (2009a).

Imidazopyridine-5,6,7,8-tetrahydro-8-quinolinamine derivatives with potent activity against HIV-1. Bioorg Med Chem Lett 19: 6399–6403.

Gudmundsson KS, Sebahar PR, Richardson L, Miller JF, Turner EM, Catalano JG *et al.* (2009b). Amine substituted N-(1H-benzimidazol-2ylmethyl)-5,6,7,8-tetrahydro-8-quinolinamines as CXCR4 antagonists with potent activity against HIV-1. Bioorg Med Chem Lett 19: 5048–5052.

Gupta SK, Pillarisetti K, Thomas RA, Aiyar N (2001). Pharmacological evidence for complex and multiple site interaction of CXCR4 with SDF-1α: implications for development of selective CXCR4 antagonists. Immunol Lett 78: 29–34.

Hatse S, Princen K, De Clercq E, Rosenkilde MM, Schwartz TW, Hernandez-Abad PE *et al.* (2005). AMD3465, a monomacrocyclic CXCR4 antagonist and potent HIV entry inhibitor. Biochem Pharmacol 70: 752–761.

Kawatkar SP, Yan M, Gevariya H, Lim MY, Eisold S, Zhu X *et al.* (2011). Computational analysis of the structural mechanism of inhibition of chemokine receptor CXCR4 by small molecule antagonists. Exp Biol Med (Maywood) 236: 844–850.

Kissow H, Hartmann B, Holst JJ, Viby N-E, Hansen LS, Rosenkilde MM *et al.* (2012). Glucagon-like peptide-1 (GLP-1) receptor agonism or DPP-4 inhibition does not accelerate neoplasia in carcinogen treated mice. Regul Pept 179: 91–100.

Kobayashi K, Oishi S, Hayashi R, Tomita K, Kubo T, Tanahara N *et al.* (2012). Structure-activity relationship study of a CXC chemokine receptor type 4 antagonist, FC131, using a series of alkene dipeptide isosteres. J Med Chem 55: 2746–2757.

Kostenis E, Zeng FY, Wess J (1998). Functional characterization of a series of mutant G protein α_q subunits displaying promiscuous receptor coupling properties. J Biol Chem 273: 17886–17892.

Ludeman JP, Stone MJ (2013). The structural role of receptor tyrosine sulfation in chemokine recognition. Br J Pharmacol 171: 1167–1179.

Maeda K, Das D, Ogata-Aoki H, Nakata H, Miyakawa T, Tojo Y *et al.* (2006). Structural and molecular interactions of CCR5 inhibitors with CCR5. J Biol Chem 281: 12688–12698.

Micallef IN, Stiff PJ, DiPersio JF, Maziarz RT, McCarty JM, Bridger G *et al.* (2009). Successful stem cell remobilization using plerixafor (mozobil) plus granulocyte colony-stimulating factor in patients with non-hodgkin lymphoma: results from the plerixafor NHL phase 3 study rescue protocol. Biol Blood Marrow Transplant 15: 1578–1586.

Miller JF, Gudmundsson KS, Aurora D, Richardson L, Jenkinson S, Spaltenstein A *et al.* (2010). Synthesis and SAR of novel isoquinoline CXCR4 antagonists with potent anti-HIV activity. Bioorg Med Chem Lett 20: 3026–3030.

Mungalpara J, Thiele S, Eriksen Ø, Eksteen J, Rosenkilde MM, Våbenø J (2012). Rational design of conformationally constrained cyclopentapeptide antagonists for C-X-C chemokine receptor 4 (CXCR4). J Med Chem 55: 10287–10291.

Mungalpara J, Zachariassen ZG, Thiele S, Rosenkilde MM, Våbenø J (2013). Structure-activity relationship studies of the aromatic positions in cyclopentapeptide CXCR4 antagonists. Org Biomol Chem 11: 8202–8208.

Murphy PM, Baggiolini M, Charo IF, Hébert CA, Horuk R, Matsushima K *et al.* (2000). International union of pharmacology. XXII. Nomenclature for chemokine receptors. Pharmacol Rev 52: 145–176.

Palczewski K, Kumasaka T, Hori T, Behnke CA, Motoshima H, Fox BA *et al.* (2000). Crystal structure of rhodopsin: a G protein-coupled receptor. Science 289: 739–745.

Pawson AJ, Sharman JL, Benson HE, Faccenda E, Alexander SP, Buneman OP *et al.*; NC-IUPHAR (2014). The IUPHAR/BPS Guide to PHARMACOLOGY: an expert-driven knowledge base of drug targets and their ligands. Nucl. Acids Res. 42 (Database Issue): D1098–1106.

Rosenkilde MM, Schwartz TW (2006). GluVII:06 – a highly conserved and selective anchor point for non-peptide ligands in chemokine receptors. Curr Top Med Chem 6: 1319–1333.

Rosenkilde MM, Cahir M, Gether U, Hjorth SA, Schwartz TW (1994). Mutations along transmembrane segment II of the NK-1 receptor affect substance P competition with non-peptide antagonists but not substance P binding. J Biol Chem 269: 28160–28164.

Rosenkilde MM, Gerlach L-O, Jakobsen JS, Skerlj RT, Bridger GJ, Schwartz TW (2004). Molecular mechanism of AMD3100 antagonism in the CXCR4 receptor: transfer of binding site to the CXCR3 receptor. J Biol Chem 279: 3033–3041.

Rosenkilde MM, Gerlach L-O, Hatse S, Skerlj RT, Schols D, Bridger GJ *et al.* (2007). Molecular mechanism of action of monocyclam versus bicyclam non-peptide antagonists in the CXCR4 chemokine receptor. J Biol Chem 282: 27354–27365.

Rosenkilde MM, Benned-Jensen T, Frimurer TM, Schwartz TW (2010). The minor binding pocket: a major player in 7TM receptor activation. Trends Pharmacol Sci 31: 567–574.

Scholten DJ, Canals M, Maussang D, Roumen L, Smit MJ, Wijtmans M *et al.* (2012). Pharmacological modulation of chemokine receptor function. Br J Pharmacol 165: 1617–1643.

Schwartz TW (1994). Locating ligand-binding sites in 7TM receptors by protein engineering. Curr Opin Biotechnol 5: 434–444.

Skerlj R, Bridger G, McEachern E, Harwig C, Smith C, Wilson T *et al.* (2011). Synthesis and SAR of novel CXCR4 antagonists that are potent inhibitors of T tropic (X4) HIV-1 replication. Bioorg Med Chem Lett 21: 262–266.

Steen A, Schwartz TW, Rosenkilde MM (2009). Targeting CXCR4 in HIV cell-entry inhibition. Mini Rev Med Chem 9: 1605–1621.

Tamamura H, Xu Y, Hattori T, Zhang X, Arakaki R, Kanbara K *et al.* (1998). A low-molecular-weight inhibitor against the chemokine receptor CXCR4: a strong anti-HIV peptide T140. Biochem Biophys Res Commun 253: 877–882.

Tamamura H, Omagari A, Oishi S, Kanamoto T, Yamamoto N, Peiper SC *et al.* (2000). Pharmacophore identification of a specific CXCR4 inhibitor, T140, leads to development of effective anti-HIV agents with very high selectivity indexes. Bioorg Med Chem Lett 10: 2633–2637.

Tamamura H, Araki T, Ueda S, Wang Z, Oishi S, Esaka A *et al.* (2005a). Identification of novel low molecular weight CXCR4 antagonists by structural tuning of cyclic tetrapeptide scaffolds. J Med Chem 48: 3280–3289.

Tamamura H, Esaka A, Ogawa T, Araki T, Ueda S, Wang Z *et al.* (2005b). Structure-activity relationship studies on CXCR4 antagonists having cyclic pentapeptide scaffolds. Org Biomol Chem 3: 4392–4394.

Tan Q, Zhu Y, Li J, Chen Z, Han GW, Kufareva I *et al.* (2013). Structure of the CCR5 chemokine receptor-HIV entry inhibitor maraviroc complex. Science 341: 1387–1390.

Tanaka T, Nomura W, Narumi T, Esaka A, Oishi S, Ohashi N *et al.* (2009). Structure-activity relationship study on artificial CXCR4 ligands possessing the cyclic pentapeptide scaffold: the exploration of amino acid residues of pentapeptides by substitutions of several aromatic amino acids. Org Biomol Chem 7: 3805–3809.

Thiele S, Steen A, Jensen PC, Mokrosinski J, Frimurer TM, Rosenkilde MM (2011). Allosteric and orthosteric sites in CC chemokine receptor (CCR5), a chimeric receptor approach. J Biol Chem 286: 37543–37554.

Thiele S, Malmgaard-Clausen M, Engel-Andreasen J, Steen A, Rummel PC, Nielsen MC *et al.* (2012). Modulation in selectivity and allosteric properties of small-molecule ligands for CC-chemokine receptors. J Med Chem 55: 8164–8177.

Trent JO, Wang ZX, Murray JL, Shao W, Tamamura H, Fujii N *et al.* (2003). Lipid bilayer simulations of CXCR4 with inverse agonists and weak partial agonists. J Biol Chem 278: 47136–471344.

Våbenø J, Nikiforovich GV, Marshall GR (2006a). Insight into the binding mode for cyclopentapeptide antagonists of the CXCR4 receptor. Chem Biol Drug Des 67: 346–354.

Våbenø J, Nikiforovich GV, Marshall GR (2006b). A minimalistic 3D pharmacophore model for cyclopentapeptide CXCR4 antagonists. Biopolymers 84: 459–471.

Wong RSY, Bodart V, Metz M, Labrecque J, Bridger G, Fricker SP (2008). Comparison of the potential multiple binding modes of bicyclam, monocyclam, and noncyclam small-molecule CXC chemokine receptor 4 inhibitors. Mol Pharmacol 74: 1485–1495.

Wu B, Chien EYT, Mol CD, Fenalti G, Liu W, Katritch V *et al.* (2010). Structures of the CXCR4 chemokine GPCR with small-molecule and cyclic peptide antagonists. Science 330: 1066–1071.

Yoshikawa Y, Kobayashi K, Oishi S, Fujii N, Furuya T (2012). Molecular modeling study of cyclic pentapeptide CXCR4 antagonists: new insight into CXCR4-FC131 interactions. Bioorg Med Chem Lett 22: 2146–2150.